JAEA-Technology
2015-021
DOI:10.11484/jaea-technology-2015-021

JAEA-Technology

Irradiation Test with Silicon Ingot for NTD-Si Irradiation Technology

Noriyuki TAKEMOTO, Nataliya ROMANOVA, Nobuaki KIMURA
Shamil GIZATULIN, Takashi SAITO, Alexandr MARTYUSHOV
Darkhan NAKIPOV, Kunihiko TSUCHIYA and Petr CHAKROV

Neutron Irradiation and Testing Reactor Center
Oarai Research and Development Center
Sector of Nuclear Science Research

August 2015
Japan Atomic Energy Agency
日本原子力研究開発機構

Irradiation Test with Silicon Ingot for NTD-Si Irradiation Technology

Noriyuki TAKEMOTO, Nataliya ROMANOVA*, Nobuaki KIMURA,
Shamil GIZATULIN*, Takashi SAITO, Alexandr MARTYUSHOV*,
Darkhan NAKIPOV*, Kunihiko TSUCHIYA and Petr CHAKROV*

Neutron Irradiation and Testing Reactor Center
Oarai Research and Development Center
Sector of Nuclear Science Research
Japan Atomic Energy Agency
Oarai-machi, Higashiibaraki-gun, Ibaraki-ken

(Received June 3, 2015)

Silicon semiconductor production by neutron transmutation doping (NTD) method using the JMTR has been investigated in Neutron Irradiation and Testing Reactor Center, Japan Atomic Energy Agency in order to expand the industry use. As a part of investigations, irradiation test with a silicon ingot was planned using WWR-K in Institute of Nuclear Physics, Republic of Kazakhstan. A device rotating the ingot made with the silicon was fabricated and was installed in the WWR-K for the irradiation test. And that, a preliminary irradiation test was carried out using neutron fluence monitors to evaluate the neutronic irradiation field. Based on the result, two silicon ingots were irradiated as scheduled, and the resistivity of each irradiated silicon ingot was measured to confirm the applicability of high-quality silicon semiconductor by the NTD method (NTD-Si) to its commercial production.

Keywords : JMTR, WWR-K, Irradiation Test, Neutron Fluence Monitor, NTD-Si

*: Institute of Nuclear Physics, Republic of Kazakhstan

NTD-Si 製造技術に係るシリコンインゴット試料の照射試験

日本原子力研究開発機構原子力科学研究部門
大洗研究開発センター照射試験炉センター

竹本　紀之、Nataliya ROMANOVA*、木村　伸明、Shamil GIZATULIN*、齋藤　隆、
Alexandr MARTYUSHOV*、Darkhan NAKIPOV*、土谷　邦彦、Petr CHAKROV*

（2015 年 6 月 3 日受理）

日本原子力研究開発機構照射試験炉センターでは、産業利用拡大の観点から JMTR を活用した中性子核変換ドーピング（Neutron Transmutation Doping：NTD）法によるシリコン半導体製造を検討している。この検討の一環として、カザフスタン共和国核物理研究所（INP）との原子力科学分野における研究開発協力のための実施取決め（試験研究炉に関する原子力技術）のもとで、INP が有する WWR-K 炉を用いたシリコンインゴット試料の照射試験を行うこととした。最初に、シリコン回転装置を製作して WWR-K 炉に設置するとともに、シリコンインゴット試料の照射位置における中性子照射場の評価を行うため、フルエンスモニタを用いた予備照射試験を行った。次に、予備照射試験結果に基づき、2 本のシリコンインゴット試料の照射試験を行うとともに、照射後の試料の抵抗率等を測定し、試験研究炉を用いた高品位シリコン半導体製造の商用生産への適用性について評価を行った。

大洗研究開発センター：〒311-1393　茨城県東茨城郡大洗町成田町 4002
*：カザフスタン共和国　核物理研究所

Contents

目　次

1. Introduction

Silicon (Si) semiconductor fabricated by a neutron transmutation doping (NTD) method using ^{30}Si (n,γ) ^{31}Si reaction, called as NTD-Si, have been widely used in various industrial fields, especially for high quality semiconductor power devices. Among various areas of research reactor utilization, the NTD method for Si is one well established technology required by industry. The NTD method can provide a direct commercial income to research reactors, and is required being installed in facilities by many research reactor operators. Therefore, enhancement of availability of the NTD method by involving more research reactor facilities would reduce the burden of potential industrial partners developing another technology or material cost. Benefitting not only industry but also the research reactor community, collaboration in the NTD method is needed. The amount of the NTD-Si production is 160 ton per year [presumption in 2004][1]. In recent years, the Si semiconductors with large diameter are required for low cost production[2]. Thus, feasibility study of the Si semiconductor production facility[3] on the JMTR (the Japan Materials Testing Reactor)[4] in Neutron Irradiation and Testing Reactor Center (NITRC) in Japan Atomic Energy Agency (JAEA) has been carried out in order to produce large size diameter (8-inches) NTD-Si. In WWR-K of Institute of Nuclear Physics (INP) of Republic of Kazakhstan, which is the light water tank-type research reactor like the JMTR, several irradiation channels have been evaluated in respect to the production of the NTD-Si, and it was found to irradiate the Si ingot of up to 8-inches in diameter[5].

As a part of the investigation, irradiation test with the Si ingot for development of the NTD-Si was planned using the WWR-K in a frame of specific topics of cooperation (STC), Irradiation Technology for NTD-Si (STC No.II-4) on the implementing arrangement between National Nuclear Center of Republic of Kazakhstan and the JAEA for “Nuclear Technology on Testing/Research Reactors” in cooperation for research and development in nuclear energy and technology [6].

As for the irradiation test, the Si-rotating device[7] was fabricated in JAEA, and the fabricated device was transported with irradiation specimens from Japan to Kazakhstan. Then the device was installed in the WWR-K, and a preliminary irradiation test using fluence monitors was carried out in order to evaluate the neutronic irradiation field of the irradiation channel for the Si ingot. Based on the result, Si ingots were irradiated and of which the resistivity of each irradiated ingot was measured in Japan.

This report describes the installation of the Si-rotating device on the WWR-K, the result of the preliminary irradiation test, irradiation test with the Si ingot and its resistivity measurement after irradiation to confirm the applicability of high-quality NTD-Si to the commercial production.

2. Test schedule

The WWR-K research reactor in INP is a light-water-cooled tank-type having thermal power of 6MWt. The core height is 0.6 m, and the core diameter is 0.72 m. Irradiation tests are performed using vertical and horizontal channels. According to information exchange in the technical meetings in September, 2009 between INP and JAEA, it was concluded that irradiation of the Si ingot of 8 inches in diameter is possible in the WWR-K. However, modification of the facility partly should be needed and it takes long time. Therefore, the irradiation test with the Si ingot with 6 inches in diameter was decided among INP and JAEA because of no need for drastic modification of the facility, and the irradiation channel K-23 was selected. Planned irradiation test is composed of two kinds of tests as follows.

(1) Neutronic evaluation of irradiation field

Before the irradiation test with the Si ingot, a preliminary irradiation test using aluminum (Al) ingots was planned to evaluate the actual irradiation field of the irradiation channel for the Si ingot in the irradiation channel K-23 of the WWR-K. The dimension of the Al ingot is almost same as that of Si ingots, and fluence monitors[8)] are installed into the Al ingot to measure both fast and thermal neutron fluencies after the irradiation.

On the other hand, neutronic calculations in the irradiation field are performed by INP with the computer code of MCU-REA[9)] using Monte Carlo method and the results are compared with measurement results.

(2) Irradiation test with Si ingots

The irradiation test with the Si ingots is carried out after the preliminary irradiation test. Two kinds of single crystal Si ingots with different length are prepared by JAEA for irradiation, and transported from JAEA to INP. Specification and photographs of these Si ingots are shown in Table 1 and Fig.1, respectively. Irradiated Si ingots are transported from Kazakhstan to Japan, and resistivity measurements are carried out to confirm the applicability to the commercial production.

3. Installation of Si-rotating device

3.1 Si-rotating device

The Si-rotating device was designed and fabricated in JAEA in order to conduct the irradiation test with the Si ingot in the irradiation channel K-23 of the WWR-K. The device consists of a holder of Si ingot, a rotating motor, an up-and-down motor, a control panel, a remote control panel, etc. A conceptual diagram for the irradiation test with the Si ingot in the WWR-K is shown in Fig.2.

The holder of Si ingot works as a container with cylinder shape to store the Si ingot for irradiation. The holder is suspended by an aluminum chain. The Si ingot is stored in the holder and fastened by the spacers. Location in an axial direction of Si ingot with different height is coordinated to the same by a spacer. High purity aluminum alloy (more than 99.50 %) is used for the material of the holder and the spacer in order to avoid the activation of impurity by the thermal neutron as much as possible.

The rotating motor rotates the holder of Si ingot in order to irradiate Si ingot with axial rotating for the uniform radial neutron flux distribution. The rotating speed of the device is 2 rpm. The revolution counter is installed in the control panel in order to confirm rotating of the Si ingot outside the reactor during the reactor operation. Air sealing is installed against dew condensation because the humidity in the channel is 100 % in maximum.

The up-and-down motor transfers the holder of Si ingot in an axial direction between the irradiated and cooled locations in the channel. Air sealing is also set against dew condensation. The encoder is incorporated at the up-and-down motor to measure the height of the Si ingot, and the axial location is indicated on the location detector at the control panel.

The rotating motor and the up-and-down motor are operated using the control panel and the remote control panel. The control panel is the device for monitoring and operating the Si-rotating device. Therefore, the revolution detector and the location detector are incorporated. The remote control panel is incorporated at the laboratory with 30 m far from the reactor, and enables simple operation of the Si-rotating device without entering the reactor room. Therefore, the revolution detector and the location detector are not incorporated.

Structural design conditions in order to install the Si-rotating device on the top of the WWR-K are listed in Table 2. It is impossible to access to the device from outside the reactor during reactor operation because the top of the WWR-K is covered with a protective cover. Therefore, the space for installation of the device is limited, and the device should be operated by a remote control. The Si ingot should be irradiated at the thermal power of 6 MW and should not be irradiated during the start-up and shutdown of the reactor to uniform axial neutron flux distribution of the Si ingot.

The photograph of the fabricated Si-rotating device is shown in Fig.3. After fabrication, inspection tests such as visual inspection, dimensional inspection, number inspection, material inspection and performance verification test were performed, and it was confirmed to satisfy design conditions.

The Si-rotating device was transported from JAEA to INP with specimens such as Si and Al ingots described in chapter 4.1, and the transportation was completed at September 13th, 2011.

3.2 Operation test

The Si-rotating device was assembled in the reactor building of the WWR-K, and was set on the basement near the reactor for an operation test. After the assembly test, the operation test was carried out on September 20th and 21th, 2011 by JAEA and INP, and the results are listed in Table 3. As a result, it was confirmed to operate normally and safely.

3.3 Installation in WWR-K

The Si-rotating device was installed into the irradiation channel K-23 at the WWR-K for the installation by the crane. However during the work, it was found that the encoder and the motor cable of the rotating motor interfere with an important component for the WWR-K control on the top of the reactor. Therefore, the encoder was removed from the device with some modifications of related circuits, and the arrangement of the motor cable was changed by rewiring with agreement of JAEA and INP. Then, the Si-rotating device was installed again, and was installed successfully. After the installation, operation test was carried out, and it was also confirmed to operate normally and safely. These works were carried out on September 22th and 23rd, 2011 by JAEA and INP.

As a result of the specification change, it became to be impossible to indicate an axial location of the Si ingot on the control panel, and to use the remote control panel. Therefore, the axial location of the Si ingot is controlled by limit switches.

4. Preliminary irradiation test for evaluation of neutron irradiation field

4.1 Preparation of specimen

In order to evaluate the actual irradiation field in the irradiation channel of the Si ingot in the irradiation channel K-23 of the WWR-K, the preliminary irradiation test using fluence monitors (F/Ms) was planned.

As for F/Ms used in the JMTR, $^{54}Fe(n, p)^{54}Mn$ reaction of iron wire and $^{59}Co(n,\gamma)^{60}Co$ reaction of aluminum-cobalt (0.11wt% of cobalt) wire are used as measurement method of fast and thermal neutron flux/fluence, respectively. For the preliminary irradiation test, sixty F/Ms of the same specification as the JMTR were fabricated in JAEA, named F/M number 1 to 60. Each structure and photograph of F/Ms are shown in Fig.4 to Fig.6. F/Ms were installed into an Al ingot prepared for the irradiation test. Four Al ingots which are almost the same dimension as Si ingots were fabricated in JAEA. Two ingots of them are 150mm in diameter with 202mm length, and were named as L202-1 and L202-2. Other two ingots are 150mm in diameter with 278mm length, and were named as L278-1 and L278-2.

Al ingots were made of A1070 (99.76 %), and five holes of 3 mm in diameter were drilled in each ingot in order to install F/Ms. Four holes are at the locations at the circle of 130mm in diameter and one hole is at the center location of the Al ingot. F/Ms are installed into these holes and placed at the top, middle and bottom locations, respectively. Fifteen F/Ms were installed into each Al ingot with adjustment of those axial locations by an aluminum spacer, and each hole was covered by the bolt. The name of the specimen was punched on the top face of the ingot to identify it, and was not punched on the bottom face to distinguish the top face with the bottom face. Photograph of the Al ingot is shown in Fig.7 as an example, and loading location of F/Ms is shown in Fig.8. Each F/M is associated with its loading location. Numbering method of its loading location is shown in Fig.9, and specification of F/Ms is summarized in Table 4.

4.2 Preliminary calculation of irradiation field

Before preliminary irradiation test, distribution of the thermal neutron flux density over Si ingot was calculated in INP in case that the Si ingot is located in the irradiation channel K-23 of the WWR-K. The irradiation channel K-23 is located behind the tank of active core, and the height is 5220 mm, from the top to the center core 510 mm and the bottom of channel 824 mm below the center of the core. Calculations were performed using the code MCU-REA in three-dimensional geometry of the core. The layout of the calculation nodes is shown in Fig.10, and the calculated distributions of the thermal neutron flux density (E<0.465 eV) over height of the Si ingot are shown in Fig.11 and Fig.12. The average height irregularity factor is at about 1.05. From the evaluation, it was revealed that it is possible to conduct uniform irradiation of Si ingots in the irradiation channel K-23 in the WWR-K, and irradiation conditions for Al ingots were planned.

4.3 Irradiation condition

Neutron fluence is decided by the required resistivity for the NTD-Si because there is a correlation between them. The resistivity of irradiated silicon is inversely proportional to the total concentration of the produced dopants and initially existing impurities. In the NTD method, the added atoms concentration is proportional to the irradiated neutron fluence, which is a product of the neutron flux, time of irradiation with a constant neutron flux and the reaction cross-section. As the neutron cross-section varies by neutron energy, it is influenced from the neutron spectrum in the irradiation site. In the semiconductor industry, the resistivity rather than the dopant concentration is usually used. Therefore, the relationship between the resistivity and the dopant concentration should be established first. For example, it is said that the resistivity of NTD-Si ranges from about 10 to about 1000 Ω･cm[10]. Following equations[11] are used at JAEA as for the relationship between the resistivity and the dopant concentration;

$$N_P = -\frac{5\times10^{15}}{\rho_0} + \frac{5\times10^{15}}{\rho} \qquad (1)$$

$$\phi \cdot t = \frac{N_P}{N_{Si\text{-}30} \cdot \sigma_a} \quad [cm^{-2}] \qquad (2)$$

$$t = \frac{\phi \cdot t}{\phi} \quad [s] \qquad (3)$$

where,

N_P	:	Number density of the doped phosphorus in the Si ingot [atoms/cm^3]
ρ_0	:	Resistivity before irradiation [Ω･cm]
ρ	:	Resistivity after irradiation [Ω･cm]
$\varphi \cdot t$	:	Neutron fluence [cm^{-2}]
φ	:	Neutron flux [cm^{-2}･s^{-1}]
t	:	Irradiation time [s]
$N_{Si\text{-}30}$	:	Number density of ^{30}Si in the Si ingot [atoms/cm^3]

$$= \frac{\rho \cdot Na}{A} = \frac{2.34 \cdot 6.02\times10^{23}}{28.09}\times 0.030872$$
$$= 1.55\times10^{-3}\,[atms/b/cm]$$

σ_a	:	Neutron absorption cross section of ^{30}Si[cm^2] (=0.108[b] in 2200m/s) or effective cross section

As a result of the preliminary calculation and the correlation, irradiation condition for the preliminary irradiation test was planned and listed in Table 5. Axial irradiation location of each Al ingot is arranged with reflecting the result of each preliminary irradiation test.

Test procedure for the preliminary irradiation using the Si-rotating device in the WWR-K is as follows;

(1) The Al ingot with F/Ms is loaded into the holder of Si ingot.
(2) The Si-rotating device is installed into the irradiation channel K-23 in the WWR-K, and trial run of the device is carried out during reactor shutdown. After the trial run, the holder of Si ingot is arranged at the cooled location.
(3) The holder of Si ingot with the Al ingot is transferred down to the irradiation location at 6MW operation, and the ingot is irradiated for planned time with rotating.
(4) The holder of Si ingot is transferred up from the irradiated location to the cooled location after required irradiation.
(5) The irradiated Al ingot is cooled in the cooled location up to necessary cooling time.
(6) The holder of Si ingot and the Al ingot is taken out from the reactor core after that.
(7) F/Ms are removed from the Al ingot, and neutron fluxes/fluencies are evaluated in accordance with the method described in chapter 4.4.

4.4 Evaluation of neutron fluence

After irradiation, removed F/Ms from each Al ingot are dismantled, and monitor wires are taken out. Radioactivity of these monitor wires are measured with the germanium detector. The reaction rates are calculated by using radiation activities, and then, neutron fluxes/fluencies are obtained from the reaction rates and the effective neutron cross section at the F/M location.

Neutron fluence is evaluated from the radioactivity as follows [11];

$$\Phi = A \bullet \frac{G}{NMF} \bullet \frac{1}{\sigma} \bullet \frac{\sum_{j=1}^{n} t_{i_j}}{\sum (1 - e^{-\lambda t_{i_j}}) e^{-\lambda t \omega_j}} \qquad (4)$$

where,

Φ	:	Neutron fluence (cm^{-2})
A	:	Radioactivity (Bq)
G	:	Atomic weight (Fe =55,9 amu, Co=58,9 amu)
N	:	Avogadro number (6,023*10^{23})
M	:	Weight of monitoring wire (g)
F	:	Abundance ratio of (^{54}Fe and ^{59}Co) in the monitoring wire (Fe or Al-Co)
σ	:	Effective cross section (barn)
t_{ij}	:	j_{th} irradiation time (s)

λ	:	Decay constant (s^{-1})
$t_{\omega j}$	:	Cooling time after the end of j_{th} irradiation (s)
n	:	Number of irradiation (operating cycles)

Neutron flux is calculated with normalization to the reactor power[4];

$$\phi = \frac{\Phi}{t} \tag{5}$$

where,

ϕ	:	Neutron flux ($cm^{-2} \cdot s^{-1}$)
Φ	:	Neutron fluence (cm^{-2})
t	:	Effective operating time in thermal power (6 MW) of the WWR-K (s)

$$= \frac{Integralreactorpower(MW)}{6(MW)} \times 24 \times 3600(s)$$

When F/Ms are irradiated in a neutron field, the neutron capture reaction rates of ^{59}Co and ^{54}Fe in the F/Ms are given by[12];

$$R_T = \int_0^{+\infty} \phi(E) \times \sigma^{Co59}(E) \times N^{Co59} dE = N^{Co59} \times \overline{\sigma^{Co59}} \times \phi_T \tag{6}$$

$$R_F = \int_0^{+\infty} \phi(E) \times \sigma^{Fe54}(E) \times N^{Fe54} dE = N^{Fe54} \times \overline{\sigma^{Fe54}} \times \phi_F \tag{7}$$

where,

R_T	:	Reaction rate of each F/M for the ^{59}Co (s^{-1})
R_F	:	Reaction rate of each F/M for the ^{54}Fe (s^{-1})
$\overline{\sigma^{Co59}}$	:	Normalized cross section for the $^{59}Co(n,\gamma)^{60}Co$ reaction (barn)
$\overline{\sigma^{Fe54}}$	:	Normalized cross section for the 54Fe(n, p)54Mn reaction (>1MeV) (barn)
ϕ_T	:	Thermal neutron flux ($cm^{-2} \cdot s^{-1}$),
ϕ_F	:	Fast neutron flux ($cm^{-2} \cdot s^{-1}$)
N^{Co59}	:	Atomic density of ^{59}Co
N^{Fe54}	:	Atomic density of ^{54}Fe

It is possible to calculate the neutron flux and the reaction rates of each F/M by the Monte Carlo method with three dimensional model of the core, and the normalized effective cross sections for the irradiation channel of the Si ingot in the WWR-K can be estimated by[4];

Normalized cross section of ^{54}Fe (>1MeV) $$\bar{\sigma}_{1.0}=\frac{\int_0^\infty \phi(E)\sigma(E)dE}{\int_{1.0}^\infty \phi(E)dE} \qquad (8)$$

Normalized cross section of ^{59}Co (<0.683eV) $$\bar{\sigma}_{0.683}=\frac{\int_0^\infty \phi(E)\sigma(E)dE}{\int_0^{0.683} \phi(E)dE} \qquad (9)$$

4.5 Results and discussion

As for the preliminary irradiation test in the WWR-K, measured neutron fluxes/fluencies by F/Ms of each Al ingot were tentatively estimated with effective cross sections of the commonly available tables from the references[13), 14)] which are often used in the WWR-K. The estimated tentative data are listed in Table 6 to Table 9 with considering a value of an effective cross section for the ^{59}Co (37.1±1.0) barn[13)] in the energy level of less than 0.0253 eV and an effective cross section for the ^{54}Fe 106 mb[14)] in the energy level of more than 1 MeV, respectively. These data were estimated to evaluate the actual irradiation field of Al ingots tentatively, and the purpose is to decide the location in an axial direction of the Si ingot in the irradiation channel. There is little influence in the difference of energy level between less than 0.0253 eV and less than 0.683 eV on the distribution of the thermal neutron flux density.

As for the axial location of the Al ingot, the center of the Al ingot axially is below the center of the core 70mm for L202-1 and L202-2, 30mm above the center of the core for the L278-1 and 13mm above the center of the core for L278-2, respectively. These were arranged with reflecting each result of preliminary irradiation test.

Neutronic calculation of the neutron flux and the reaction rate of each F/M at L278-2 Al ingot was carried out to estimate normalized effective cross sections by MCU code. As for A,B,C and D, each F/M measurement result was compared with average neutron fluxes among A to D because of no rotating in the MCU calculation. The calculation result is listed in Table 10. The relative errors in calculating the neutron fluxes were around 1 - 4 % to the ^{59}Co (<0.683eV) and around 5 % to the of ^{54}Fe (>1MeV). On the other hand, the relative errors in calculating the reaction rates were around 5 - 6 % to the ^{59}Co (<0.683eV) and around 5 - 7 % to the of ^{54}Fe (>1MeV). The neutron flux of each F/M at L278-2 Al ingot was sorted using the measured result and also the calculated average effective cross section as the definitive ones, and the obtained data is listed in Table 11.

Distribution of measured fast and thermal neutron flux density at L278-2 Al ingot are summarized and shown in Fig. 13 and Fig. 14. In measuring the radioactivity of irradiated F/M wires by the Ge detector, the statistical errors were around 3 % to the ^{60}Co and around 4 - 6 % to the ^{54}Mn, and these error bars are also shown in Fig. 13 and Fig.14.

The average thermal neutron flux and fluence among fifteen F/Ms at L278-2 Al ingot were about 2.78×10^{12} cm^{-2}s^{-1} and 4.01×10^{12} cm^{-2}, respectively. The result was good agreement with the targeted irradiated condition listed in Table 5. It can be also said that there are good performance about radial and axial uniformity in the result of neutron flux distribution at L278-2 Al ingot.

The irregularity factors for sorted neutron fluxes/fluencies were calculated by following equation[15] and listed in Table 12;

$$k_r = \frac{\phi_{max}}{\bar{\phi}} \qquad (10)$$

where,

$\phi_{\max}$: Maximum value of the thermal neutron flux, [cm^{-2}s^{-1}]

$\bar{\phi}$: Average value of the thermal neutron flux, [cm^{-2}s^{-1}]

The minimization of irregularity factors allows receiving enough homogenous distribution of mixtures added in the result of Si irradiation. From the evaluated data, the best location of the Si ingot from holding radiation in the irradiation channel K-23 with uniformity of neutron irradiation was determined as the same axial location as that of L278-2 Al ingot. Namely, the axial location of the center of the Si ingot in the irradiation channel K-23 was also determined as 13mm above the center of the WWR-K core.

5. Irradiation test with silicon ingot

5.1 Test condition

As a result of the preliminary irradiation test for neutronic evaluation, irradiation condition for the irradiation test with the Si ingot was determined, and listed in Table 13. As for the axial location of the Si ingot, the center of the Si ingot axially in the irradiation channel K-23 was also determined as 13mm above the center of the WWR-K core.

5.2 Resistivity measurement with irradiated silicon ingot

Irradiated two Si ingots in the WWR-K core were removed from the core and cooled in the reactor building. After cooling, these were decontaminated on the sink in the controlled area in the WWR-K by INP members under the guidance of JAEA members. After confirming of no contamination, these irradiated Si ingots were packed and transported to Japan.

These ingots were cut down in increments of 50 mm axially as shown in Fig.15 after suitable heat treatment, and resistivity of five points in each axial plane of Si ingot was measured respectively to evaluate radial and axial uniformity. An axial resistivity variation (ARV)[10] and a radial resistivity gradient (RRG)[10] were calculated using measured resistivity based on the evaluation method in JIS H 0602[16] to evaluate the axial and radial uniformity. The meaning of the ARV and the RRG are as follows.

$$\mathrm{ARV}^{10)} = 100 \cdot \{\rho_{(plane\_max)} - \rho_{(plane\_min)}\} / \rho_{(plane\_min)} \text{ in } \% \qquad (11)$$

$$\mathrm{RRG}^{10)} = 100 \cdot (\rho_{max} - \rho_{min}) / \rho_{min} \text{ in } \% \qquad (12)$$

The initial resistivity and uncertainty in the resistivity measurement has an effect on the RRG directly. Above effects may be reflected in the specifications. While the specification of the RRG would depend on the customer, it is usually less than or equal to 4–5% nowadays. The requirement for axial resistivity uniformity depends on the customers and a variation RRG within 5–8% has been usually required.

5.3 Results and discussion

The irradiation test with two Si ingots was carried out, and completed as scheduled. The result of irradiation test is listed in Table 14. Then, the irradiated Si ingots were transported into Japan, and each resistivity was measured. The result of the resistivity measurement is listed in Table 15 and Table 16. As no Si spacer was set below and above the ingot in the irradiation test, the result of the top and bottom plane was ignored in the evaluation. As a result of the test, followings became clear;

(1) Uniformity in radial and axial direction

There was no problem in the stacking fault by the fast neutron in each Si ingot. As for the Si ingot No.1, axial uniformity was evaluated, and the result was very good enough level for the commercial production.

As for the Si ingot No. 2, axial and radial uniformity was evaluated. The RRG of the Si ingot No.2 was within 4.8 % and the radial uniformity was good enough level for the commercial production in this time. On the other hand, the RRG was 9.8 %, and the axial uniformity was insufficient level for the commercial production in this time. It is considered that the gradient of axial neutron flux distribution in the WWR-K core has an effect on the gradient of neutron reaction because the length of the Si ingot No.2 is longer than the Si ingot No.1. Therefore, the axial uniformity of the resistivity will be improved by application of an axial neutron flux flattening method such as an inversion method, a filter method and so on, and also by installation of the Si spacer on the top of the ingot and below the bottom of the ingot.

(2) Measured resistivity

Target resistivity was both 500 Ω･cm by 4 hours irradiation. However, the result was about 400 Ω･cm in average in the Si ingot No.2. Parametric irradiation tests in the WWR-K core will be needed to reveal the relation between irradiation time and resistivity when the commercial production is planned.

6. Summary

Irradiation test with the Si ingot was planned using the WWR-K in INP by JAEA and INP. Before the irradiation test, the fabricated Si-rotating device was established on the WWR-K, and preliminary irradiation test using Al ingots was carried out. As a result, the irradiation field was evaluated, and the test condition of the Si ingot was determined. Si ingots were irradiated as scheduled, and the resistivity of each irradiated ingot was measured. It can be said to be possible to apply the light-water-cooled tank-type reactor such as the WWR-K and the JMTR to the commercial production of the NTD-Si. On the other hand, it is indispensable to apply the axial neutron flux flattening method to meet the criteria of the commercial production and to perform parametric irradiation tests to know the relation between irradiation time and the resistivity in each site. The uniformity of neutron irradiation is usually expressed by radial and axial uniformities. The principle to achieve uniform irradiation is rather simple, and the methods can be classified into a few types. However, even when the same method is used, the design and operation of an NTD facility can vary greatly depending on the circumstances of each irradiation site. Therefore, it is recommended that a reactor starting an NTD project should search for the appropriate method by considering the characteristics and conditions of their own reactor, rather than imitating an example.

Acknowledgements

Authors express gratefully appreciate for helpful comments on this paper by Dr. H. Kawamura (Director General, Fukushima Research Infrastructural Creation Center, JAEA), Mr. Y. Nagao (General Manager, Fukushima Research Infrastructural Creation Center, JAEA) and Dr. S. Ueta (Assistant Principal Researcher, Nuclear Hydrogen and Heat Application Research Center, JAEA) and Mr. Takeshi Nakajima (Sangyo Kagaku Co., LTD).

References

1) Working Group for NTD Technology: "Expansion of Neutron-Transmutation-Doped Silicon (NTD-Si) Semiconductor Productivity using Research Reactors (JRR-3, JRR-4, and JMTR)", JAEA-Review 2005-006, (2006), 56p. [in Japanese]
2) C. H. Carter et al. : "Current Status of Large Diameter, Low Defect SiC Boule Growth", Future Electron Device Journal Vol.11 No.2, pp.7-10 (2000).
3) J. Hosokawa et al. : "Conceptual Study of Silicon Semiconductor Production Facility in JMTR", JAEA-Technology 2008-038, (2008), 24p. [in Japanese]
4) Department of JMTR Project: " JMTR Irradiation Handbook", JAERI-M 94-023, (1994). [in Japanese]
5) P. Chakrov et al. : "WWR-K Research Reactor –Status and Future Plans", Proceedings of the International Symposium on Materials Testing Reactors, JAEA-Conf 2008-011, pp.35-41 (2008).
6) H. Kawamura et al. : "Status of International Cooperation in Nuclear Technology on Testing/Research Reactors between JAEA and INP-NNC", JAEA-Review 2011-042, (2011), 46p.
7) N. Kimura et al. : "Design, Fabrication and Transportation of Si Rotating Device", JAEA-Technology 2012-012, (2012), 34p. [in Japanese]
8) Y. Nagao et al. : "JMTR Strategy of Restart and Dosimetry for Standardization of Irradiation Technology", JAEA-Conf 2008-011, pp. 73-77 (2008).
9) Program MCU-REA with library of nuclear constants DLC/MCUDAT-2.1. Problems of Atomic Science and Engineering. Series: Physics of Nuclear Reactor. Moscow, 2001. issue 3, pp.55-62, (2001)[in Russian]
10) International Atomic Energy Agency: "Neutron Transmutation Doping of Silicon at Research Reactors", IAEA-TECDOC-1681, (2012).
11) M. Yagi et al. : "Conceptual Design of Irradiation Experimental Device for 12 inch NTD-Si Ingot in JRR-4", JAEA-Technology 2008-015, (2008), 91p. [in Japanese]
12) Lamarsh, J.R. : "Introduction to Nuclear Reactor Theory", Addison-Wesley, New York, (1996), 598 p.

13) K.H. Beckurts and K. Wirtz : "Neutron Physics" Springer-Verlag Berlin-Göttingen-Heidelberg-New York, (1964).
14) Helm J.L. : "Investigations into power reactor fluence uncertainties and their implications for trend curves", Reactor Dosimetry. ASTM STR 1228. Harry Farrar, etc., American Society For Testing And Materials, Philadelphia, (1994).
15) Dementev B.A. : " Nuclear power of reactors", Moscow, pp.107-108, (1984). [in Russian]
16) Japanese Industrial Standards Committee: "JIS H 0602:1995, Testing method of resistivity for silicon crystals and silicon wafers with four-point probe".

Table 1　Specification of Si ingot

No	Diameter [mm]	Length [mm]	Weight [kg]
1	151.13	202	8,443
2	151.14	278	11,621

Table 2　Design condition for Si-rotating device in WWR-K

	Item	condition
Top of core	Atmosphere	Air
	Humidity	100%
Irradiation channel (K-23)	Height (Max.)	4.900m
	Internal diameter	193mm
	Atmosphere	Coolant water / Air
	Coolant water level	At least 2 m above the top of the effective core
	Coolant water temperature	about 45˚C
	Coolant water flow	No
Power source	In-core	Less than 48V (AC50Hz / DC)
	Ex-core	220V (AC50Hz / DC)

Table 3 Operation test of Si-rotating device

Operation test using control panel		
Inspection item	Criterion	Result
Winch Up	Winch up Stop at upper limit Winch speed (1m±10cm/min)	Up Stop at upper limit 65s/m
Winch Down	Winch down Stop at lower limit Winch speed (1m±10cm/min)	Down Stop at lower limit 65s/m
Emergency	Stop winching up when pushing emergency Stop winching down when pushing emergency	Stop Stop
Rotation On	Rotation On Rotation Off Rotation speed (2rpm±10%rpm)	On Off 118s/2rpm
Emergency	Stop rotating when pushing emergency	Stop
Operation test using remote control panel		
Inspection item	Criterion	Result
Winch Up	Winch up Stop at upper limit	Up Stop at upper limit
Winch Down	Winch down Stop at lower limit	Down Stop at lower limit
Emergency	Stop winching up when pushing emergency Stop winching down when pushing emergency	Stop Stop
Rotation On	Rotation On Rotation Off	On Off
Emergency	Stop rotating when pushing emergency	Stop

Table 4 List of fluence monitors (1/2)

Number for loading		Number of F/M	Weight of F/M (g)	Fe		Al-0.475%Co	
				W (mg)	Length (mm) × number	W (mg)	Length (mm)
L202-1-	A-1	1	0.16	8.182	5×5	1.326	1
	A-2	2	0.17	7.990	5×5	1.482	1
	A-3	3	0.16	8.310	5×5	1.258	1
	B-1	4	0.17	8.106	5×5	1.281	1
	B-2	5	0.17	8.167	5×5	1.055	1
	B-3	6	0.17	7.988	5×5	1.504	1
	C-1	7	0.17	8.108	5×5	1.127	1
	C-2	8	0.17	8.045	5×5	1.253	1
	C-3	9	0.17	8.166	5×5	1.370	1
	D-1	10	0.16	8.111	5×5	1.563	1
	D-2	11	0.18	8.061	5×5	1.337	1
	D-3	12	0.17	8.220	5×5	1.212	1
	E-1	13	0.16	8.134	5×5	1.115	1
	E-2	14	0.17	8.117	5×5	1.459	1
	E-3	15	0.17	8.121	5×5	1.230	1
L202-2-	A-1	16	0.17	8.070	5×5	1.330	1
	A-2	17	0.17	8.334	5×5	1.322	1
	A-3	18	0.17	8.210	5×5	1.115	1
	B-1	19	0.16	7.943	5×5	1.581	1
	B-2	20	0.17	8.178	5×5	1.281	1
	B-3	21	0.16	7.990	5×5	1.233	1
	C-1	22	0.17	7.902	5×5	1.389	1
	C-2	23	0.17	8.113	5×5	1.381	1
	C-3	24	0.17	7.958	5×5	1.512	1
	D-1	25	0.17	8.238	5×5	1.315	1
	D-2	26	0.16	8.095	5×5	1.329	1
	D-3	27	0.17	8.248	5×5	1.320	1
	E-1	28	0.17	8.159	5×5	1.098	1
	E-2	29	0.17	8.129	5×5	1.064	1
	E-3	30	0.17	8.150	5×5	1.183	1

Table 4 List of fluence monitors (2/2)

Numbering for loading		Number of F/M	Weight of F/M (g)	Fe		Al-0.475%Co	
				W (mg)	Length (mm) × number	W (mg)	Length (mm)
L278-1-	A-1	31	0.17	8.167	5×5	1.119	1
	A-2	32	0.17	8.184	5×5	1.271	1
	A-3	33	0.17	7.877	5×5	1.103	1
	B-1	34	0.17	8.113	5×5	1.187	1
	B-2	35	0.17	8.221	5×5	1.218	1
	B-3	36	0.17	7.952	5×5	1.103	1
	C-1	37	0.17	7.986	5×5	1.198	1
	C-2	38	0.17	8.208	5×5	1.301	1
	C-3	39	0.17	8.128	5×5	1.228	1
	D-1	40	0.16	8.033	5×5	0.950	1
	D-2	41	0.16	8.096	5×5	1.150	1
	D-3	42	0.17	8.374	5×5	1.132	1
	E-1	43	0.16	8.208	5×5	1.071	1
	E-2	44	0.17	8.019	5×5	1.493	1
	E-3	45	0.17	8.093	5×5	1.410	1
L278-2-	A-1	46	0.17	8.053	5×5	1.272	1
	A-2	47	0.16	8.162	5×5	1.036	1
	A-3	48	0.17	8.106	5×5	1.126	1
	B-1	49	0.17	8.005	5×5	1.340	1
	B-2	50	0.17	8.334	5×5	1.079	1
	B-3	51	0.17	7.949	5×5	1.081	1
	C-1	52	0.17	8.042	5×5	1.154	1
	C-2	53	0.17	8.026	5×5	1.132	1
	C-3	54	0.17	7.953	5×5	1.247	1
	D-1	55	0.17	8.200	5×5	1.184	1
	D-2	56	0.17	7.942	5×5	1.201	1
	D-3	57	0.17	8.187	5×5	1.156	1
	E-1	58	0.17	7.915	5×5	0.991	1
	E-2	59	0.17	8.107	5×5	1.112	1
	E-3	60	0.17	7.981	5×5	1.278	1

Table 5 Irradiation condition for preliminary irradiation test

Test No.	Name of specimen	Rotation	Thermal neutron fluence [cm^{-2}]	Thermal neutron flux [$cm^{-2}\cdot s^{-1}$]	Irradiation time [h]
I-1	L202-1	2rpm	2×10^{16}	2.8×10^{12}	2
I-2	L202-2	2rpm	4×10^{16}	2.8×10^{12}	4
I-3	L278-1	2rpm	2×10^{16}	2.8×10^{12}	2
I-4	L278-2	2rpm	4×10^{16}	2.8×10^{12}	4

Table 6 Tentative data of neutron flux/fluence for L202-1 Al ingot

Loading location	Number of F/M	Neutron fluence (cm^{-2})		Neutron flux ($cm^{-2}s^{-1}$)	
		Fast [>1 MeV]	Thermal [<0.683eV]	Fast [>1 MeV]	Thermal [<0.683eV]
L202-1-A-1	1	1.54×10^{15}	2.09×10^{16}	2.14×10^{11}	2.88×10^{12}
L202-1-A-2	2	1.65×10^{15}	7.89×10^{15}	2.29×10^{11}	1.08×10^{12}
L202-1-A-3	3	1.25×10^{15}	1.79×10^{16}	1.74×10^{11}	2.45×10^{12}
L202-1-B-1	4	1.52×10^{15}	—*	2.11×10^{11}	—*
L202-1-B-2	5	1.45×10^{15}	1.99×10^{16}	2.02×10^{11}	2.73×10^{12}
L202-1-B-3	6	1.11×10^{15}	1.76×10^{16}	1.54×10^{11}	2.42×10^{12}
L202-1-C-1	7	1.50×10^{15}	2.19×10^{16}	2.09×10^{11}	3.01×10^{12}
L202-1-C-2	8	1.36×10^{15}	1.98×10^{16}	1.89×10^{11}	2.72×10^{12}
L202-1-C-3	9	1.18×10^{15}	1.80×10^{16}	1.64×10^{11}	2.47×10^{12}
L202-1-D-1	10	1.62×10^{15}	2.13×10^{16}	2.25×10^{11}	2.93×10^{12}
L202-1-D-2	11	1.47×10^{15}	1.89×10^{16}	2.05×10^{11}	2.59×10^{12}
L202-1-D-3	12	1.13×10^{15}	1.84×10^{16}	1.57×10^{11}	2.52×10^{12}
L202-1-E-1	13	1.55×10^{15}	1.97×10^{16}	2.15×10^{11}	2.71×10^{12}
L202-1-E-2	14	1.42×10^{15}	1.92×10^{16}	1.97×10^{11}	2.64×10^{12}
L202-1-E-3	15	1.12×10^{15}	1.67×10^{16}	1.56×10^{11}	2.29×10^{12}

*: missing

Table 7 Tentative data of neutron flux/fluence for L202-2 Al ingot

Loading location	Number of F/M	Neutron fluence (cm^{-2})		Neutron flux ($cm^{-2}s^{-1}$)	
		Fast [>1 MeV]	Thermal [<0.683eV]	Fast [>1 MeV]	Thermal [<0.683eV]
L202-2-A-1	16	3.42×10^{15}	4.35×10^{16}	2.26×10^{11}	2.99×10^{12}
L202-2-A-2	17	3.26×10^{15}	4.08×10^{16}	2.16×10^{11}	2.81×10^{12}
L202-2-A-3	18	2.87×10^{15}	3.87×10^{16}	1.90×10^{11}	2.66×10^{12}
L202-2-B-1	19	3.36×10^{15}	4.38×10^{16}	2.13×10^{11}	3.02×10^{12}
L202-2-B-2	20	3.21×10^{15}	4.15×10^{16}	2.02×10^{11}	2.86×10^{12}
L202-2-B-3	21	2.74×10^{15}	3.65×10^{16}	1.78×10^{11}	2.51×10^{12}
L202-2-C-1	22	3.30×10^{15}	4.21×10^{16}	2.18×10^{11}	2.90×10^{12}
L202-2-C-2	23	3.11×10^{15}	4.27×10^{16}	2.05×10^{11}	2.94×10^{12}
L202-2-C-3	24	2.59×10^{15}	3.77×10^{16}	1.71×10^{11}	2.59×10^{12}
L202-2-D-1	25	3.41×10^{15}	2.62×10^{16}	2.22×10^{11}	1.80×10^{12}
L202-2-D-2	26	3.29×10^{15}	4.30×10^{16}	2.17×10^{11}	2.96×10^{12}
L202-2-D-3	27	2.93×10^{15}	4.00×10^{16}	1.93×10^{11}	2.75×10^{12}
L202-2-E-1	28	3.15×10^{15}	4.03×10^{16}	2.05×10^{11}	2.77×10^{12}
L202-2-E-2	29	3.25×10^{15}	3.97×10^{16}	2.12×10^{11}	2.73×10^{12}
L202-2-E-3	30	2.47×10^{15}	3.62×10^{16}	1.61×10^{11}	2.49×10^{12}

Table 8 Tentative data of neutron flux/fluence for L278-1 Al ingot

Loading location	Number of F/M	Neutron fluence (cm^{-2})		Neutron flux ($cm^{-2}s^{-1}$)	
		Fast [>1 MeV]	Thermal [<0.683eV]	Fast [>1 MeV]	Thermal [<0.683eV]
L278-1-A-1	31	9.78×10^{14}	—*	1.36×10^{11}	—*
L278-1-A-2	32	1.37×10^{15}	1.96×10^{16}	1.90×10^{11}	2.69×10^{12}
L278-1-A-3	33	1.45×10^{15}	2.13×10^{16}	2.02×10^{11}	2.93×10^{12}
L278-1-B-1	34	1.06×10^{15}	—*	1.47×10^{11}	—*
L278-1-B-2	35	1.40×10^{15}	1.87×10^{16}	1.94×10^{11}	2.57×10^{12}
L278-1-B-3	36	1.33×10^{15}	2.13×10^{16}	1.85×10^{11}	2.93×10^{12}
L278-1-C-1	37	1.10×10^{15}	1.62×10^{16}	1.53×10^{11}	2.22×10^{12}
L278-1-C-2	38	1.44×10^{15}	1.85×10^{16}	2.01×10^{11}	2.54×10^{12}
L278-1-C-3	39	1.40×10^{15}	1.83×10^{16}	1.95×10^{11}	2.52×10^{12}
L278-1-D-1	40	1.00×10^{15}	1.58×10^{16}	1.39×10^{11}	2.17×10^{12}
L278-1-D-2	41	1.50×10^{15}	1.90×10^{16}	2.09×10^{11}	2.61×10^{12}
L278-1-D-3	42	1.53×10^{15}	—*	2.13×10^{11}	—*
L278-1-E-1	43	9.07×10^{14}	1.58×10^{16}	1.26×10^{11}	2.18×10^{12}
L278-1-E-2	44	—*	—*	—*	—*
L278-1-E-3	45	1.55×10^{15}	2.66×10^{16}	2.15×10^{11}	3.66×10^{12}

*: missing

Table 9 Tentative data of neutron flux/fluence for L278-2 Al ingot

Loading location	Number of F/M	Neutron fluence (cm^{-2})		Neutron flux ($cm^{-2}s^{-1}$)	
		Fast [>1 MeV]	Thermal [<0.683eV]	Fast [>1 MeV]	Thermal [<0.683eV]
L278-2-A-1	46	2.37×10^{15}	3.90×10^{16}	1.64×10^{11}	2.71×10^{12}
L278-2-A-2	47	3.12×10^{15}	4.00×10^{16}	2.17×10^{11}	2.78×10^{12}
L278-2-A-3	48	3.12×10^{15}	4.20×10^{16}	2.16×10^{11}	2.92×10^{12}
L278-2-B-1	49	2.44×10^{15}	3.97×10^{16}	1.69×10^{11}	2.75×10^{12}
L278-2-B-2	50	2.44×10^{15}	4.30×10^{16}	2.21×10^{11}	2.98×10^{12}
L278-2-B-3	51	2.95×10^{15}	4.38×10^{16}	2.05×10^{11}	3.04×10^{12}
L278-2-C-1	52	2.20×10^{15}	3.79×10^{16}	1.53×10^{11}	2.63×10^{12}
L278-2-C-2	53	3.12×10^{15}	4.01×10^{16}	2.16×10^{11}	2.78×10^{12}
L278-2-C-3	54	2.66×10^{15}	4.13×10^{16}	1.85×10^{11}	2.87×10^{12}
L278-2-D-1	55	2.41×10^{15}	3.73×10^{16}	1.68×10^{11}	2.59×10^{12}
L278-2-D-2	56	2.63×10^{15}	4.04×10^{16}	1.82×10^{11}	2.81×10^{12}
L278-2-D-3	57	2.70×10^{15}	4.15×10^{16}	1.87×10^{11}	2.88×10^{12}
L278-2-E-1	58	2.34×10^{15}	3.74×10^{16}	1.62×10^{11}	2.60×10^{12}
L278-2-E-2	59	2.91×10^{15}	4.02×10^{16}	2.02×10^{11}	2.79×10^{12}
L278-2-E-3	60	2.70×10^{15}	4.10×10^{16}	1.88×10^{11}	2.85×10^{12}

Table 10 Calculated neutron flux/reaction rate for L278-2 Al ingot

Loading location	Number of F/M	Neutron flux ($cm^{-2}s^{-1}$)		Reaction rate (s^{-1})	
		Fast [>1 MeV]	Thermal [<0.683eV]	^{54}Fe [>1 MeV]	^{59}Co [<0.683eV]
L278-2-A-1	46	5.12×10^{10}	1.83×10^{12}	7.70×10^{09}	7.20×10^{13}
L278-2-A-2	47	7.94×10^{10}	2.18×10^{12}	9.14×10^{09}	8.13×10^{13}
L278-2-A-3	48	6.01×10^{10}	1.97×10^{12}	8.00×10^{09}	7.35×10^{13}
L278-2-B-1	49	1.34×10^{11}	2.34×10^{12}	1.38×10^{10}	8.72×10^{13}
L278-2-B-2	50	1.66×10^{11}	2.53×10^{12}	1.52×10^{10}	9.35×10^{13}
L278-2-B-3	51	1.44×10^{11}	2.39×10^{12}	1.44×10^{10}	8.77×10^{13}
L278-2-C-1	52	5.39×10^{11}	4.46×10^{12}	2.71×10^{10}	1.70×10^{14}
L278-2-C-2	53	5.62×10^{11}	4.76×10^{12}	2.51×10^{10}	1.78×10^{14}
L278-2-C-3	54	5.59×10^{11}	4.55×10^{12}	2.74×10^{10}	1.73×10^{14}
L278-2-D-1	55	1.26×10^{11}	2.30×10^{12}	1.33×10^{10}	8.59×10^{13}
L278-2-D-2	56	1.63×10^{11}	2.54×10^{12}	1.47×10^{10}	9.51×10^{13}
L278-2-D-3	57	1.38×10^{11}	2.34×10^{12}	1.40×10^{10}	8.86×10^{13}
L278-2-E-1	58	1.54×10^{11}	2.67×10^{12}	1.62×10^{10}	9.83×10^{13}
L278-2-E-2	59	2.05×10^{11}	2.82×10^{12}	1.87×10^{10}	1.05×10^{14}
L278-2-E-3	60	1.59×10^{11}	2.73×10^{12}	1.42×10^{10}	9.93×10^{13}
Ave*-1	-	2.12×10^{11}	2.73×10^{12}	1.55×10^{10}	1.04×10^{14}
Ave*-2	-	2.43×10^{11}	3.00×10^{12}	1.60×10^{10}	1.12×10^{14}
Ave*-3	-	2.25×10^{11}	2.81×10^{12}	1.60×10^{10}	1.06×10^{14}
Ingot ave.	-	2.04×10^{11}	2.84×10^{12}		

Ave*: Average among A, B, C and D

Table 11 Definitive data of neutron flux/fluence for L278-2 Al ingot

Loading location	Number of F/M	Neutron fluence (cm^{-2})		Neutron flux ($cm^{-2}s^{-1}$)	
		Fast [>1 MeV]	Thermal [<0.683eV]	Fast [>1 MeV]	Thermal [<0.683eV]
L278-2-A-1	46	3.14×10^{15}	3.88×10^{16}	2.18×10^{11}	2.69×10^{12}
L278-2-A-2	47	4.77×10^{15}	3.98×10^{16}	3.31×10^{11}	2.77×10^{12}
L278-2-A-3	48	4.35×10^{15}	4.18×10^{16}	3.02×10^{11}	2.90×10^{12}
L278-2-B-1	49	3.24×10^{15}	3.94×10^{16}	2.25×10^{11}	2.74×10^{12}
L278-2-B-2	50	4.85×10^{15}	4.28×10^{16}	3.37×10^{11}	2.97×10^{12}
L278-2-B-3	51	4.12×10^{15}	4.35×10^{16}	2.86×10^{11}	3.02×10^{12}
L278-2-C-1	52	2.93×10^{15}	3.76×10^{16}	2.03×10^{11}	2.61×10^{12}
L278-2-C-2	53	4.76×10^{15}	3.99×10^{16}	3.30×10^{11}	2.77×10^{12}
L278-2-C-3	54	3.71×10^{15}	4.11×10^{16}	2.58×10^{11}	2.85×10^{12}
L278-2-D-1	55	3.21×10^{15}	3.70×10^{16}	2.23×10^{11}	2.57×10^{12}
L278-2-D-2	56	4.01×10^{15}	4.03×10^{16}	2.79×10^{11}	2.80×10^{12}
L278-2-D-3	57	3.76×10^{15}	4.13×10^{16}	2.61×10^{11}	2.87×10^{12}
L278-2-E-1	58	2.57×10^{15}	3.72×10^{16}	1.79×10^{11}	2.58×10^{12}
L278-2-E-2	59	3.62×10^{15}	3.99×10^{16}	2.52×10^{11}	2.77×10^{12}
L278-2-E-3	60	3.23×10^{15}	4.08×10^{16}	2.24×10^{11}	2.83×10^{12}

Table 12 Irregularity factor for preliminary irradiation test

Al ingot L 202-1*		Al ingot L 202-2*		Al ingot L 278-1*		Al ingot L 278-2	
Height		Height		Height		Height	
K_zA	1.08	K_zA	1.06	K_zA	1.04	K_zA	1.04
K_zB	1.06	K_zB	1.08	K_zB	1.07	K_zB	1.04
K_zC	1.10	K_zC	1.05	K_zC	1.05	K_zC	1.04
K_zD	1.09	K_zD	1.04	K_zD	1.09	K_zD	1.04
K_zE	1.06	K_zE	1.04	K_zE	1.00	K_zE	1.04
Radius		Radius		Radius		Radius	
K_rAEC1	1.05	K_rAEC1	1.04	K_rAEC1	1.01	K_rAEC1	1.02
K_rAEC2	1.02	K_rAEC2	1.04	K_rAEC2	1.03	K_rAEC2	1.00
K_rAEC3	1.03	K_rAEC3	1.03	K_rAEC3	1.08	K_rAEC3	1.01
K_rDEB1	1.04	K_rDEB1	1.04	K_rDEB1	1.00	K_rDEB1	1.04
K_rDEB2	1.03	K_rDEB2	1.04	K_rDEB2	1.01	K_rDEB2	1.04
K_rDEB3	1.05	K_rDEB3	1.07	K_rDEB3	1.00	K_rDEB3	1.04
Volume		Volume		Volume		Volume	
1.14		1.08		1.16		1.09	

*: To be exception maximum deviation

Table 13　Irradiation condition of silicon ingot

Test No.	Name of specimen	Rotation	Thermal neutron fluence [cm^{-2}]	Thermal neutron flux [$cm^{-2} \cdot s^{-1}$]	Irradiation time [h]
II-1	No.1 (202mmL)	2rpm	4×10^{16}	2.8×10^{12}	4
II-2	No.2 (278mmL)	2rpm	4×10^{16}	2.8×10^{12}	4

Table 14　Irradiation test result with silicon ingot

Item	Silicon ingot No.1	Silicon ingot No.2
Irradiation channel	K-23	K-23
Axial location	+13 mm [from the core center]	+13 mm [from the core center]
Irradiation date	Feb. 27th, 2013 13:15 to 17:15	Apr. 9, 2013 09:30 to 13:30
Irradiation time	4 hours	4 hours
Irradiation temperature	30.51-37.79℃ (Light water)	35.28-42.46℃ (Light water)
Number of rotation	2 rpm	2 rpm
Inversion of specimen	No	No
Si spacer	No	No

Table 15 Result of resistivity measurement with silicon ingot No.1

<Uniformity in axial direction>

Measured point	Resistivity (Mean) [Ω･cm]	A to E			B to D*		
		Max.	Min.	ARV	Max.	Min.	ARV
A – A plane	448.3	448.3	424.6	5.6 %	429.3	424.6	1.1 %
B – B plane	429.3						
C – C plane	424.6						
D –D plane	425.3						
E – E plane	431.0						

*: There is no Si spacer below and above the ingot in this test. Therefore, data of A-A plane and D-D plane were ignored for the evaluation.

Table 16 Result of resistivity measurement with silicon ingot No.2

< Uniformity in axial direction >

Measured point	Resistivity (Mean) [Ω･cm]	A to F			B to E*		
		Max.	Min.	ARV	Max.	Min.	ARV
A – A plane	425.1	425.1	378.3	12.4 %	415.5	378.3	9.8 %
B – B plane	415.5						
C – C plane	387.3						
D –D plane	379.7						
E – E plane	378.3						
F – F plane	382.7						

*: There is no Si spacer below and above the ingot in this test. Therefore, data of A-A plane and E-E plane were ignored for the evaluation.

< Uniformity in radial direction >

Measured point	Resistivity [Ω･cm]					Max.	Min.	RRG*
	R1	R2	R3	R4	R5			
A – A plane	436.6	426.7	420.6	421.7	428.6	436.6	419.2	4.2 %
B – B plane	411.6	411.5	423.8	408.3	405.5	424.0	405.5	4.6 %
C – C plane	389.8	390.5	388.1	384.1	382.1	390.5	382.1	2.2 %
D –D plane	368.0	380.5	384.7	381.4	374.1	385.5	368.0	4.8 %
E – E plane	370.8	377.9	381.8	379.9	374.3	382.1	370.8	3.0 %
F – F plane	374.6	383.8	391.7	378.2	367.3	392.0	367.3	6.7 %

*: There is no Si spacer below and above the ingot in this test. Therefore, data of A-A plane and E-E plane were ignored for the evaluation.

(1) Silicon ingot No. 1
(ϕ151mm×202mmL)

(2) Silicon ingot No.2
(ϕ151mm×278mmL)

Fig.1 Photograph of silicon ingot

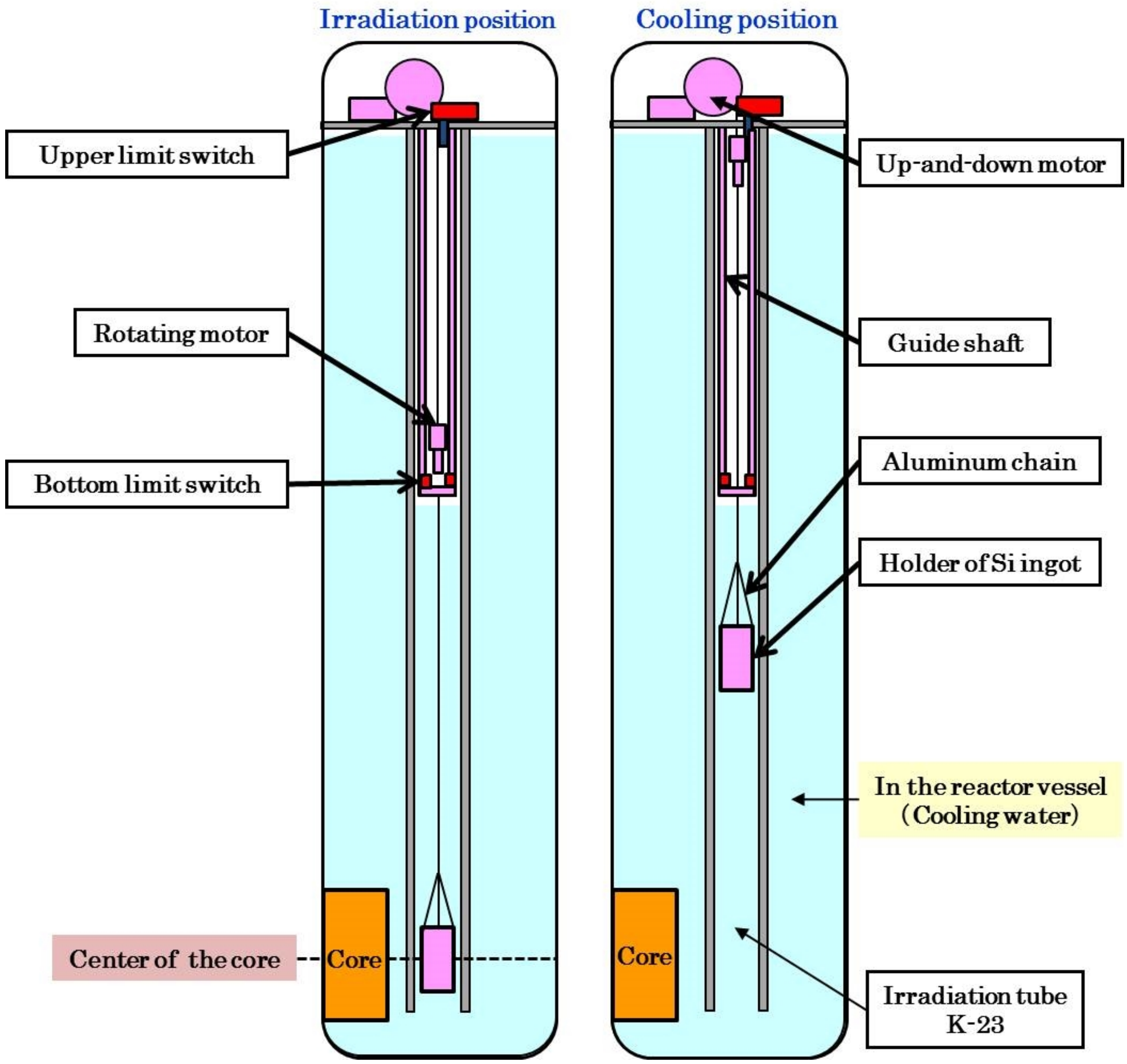

Fig.2 Conceptual diagram for irradiation test with silicon ingot

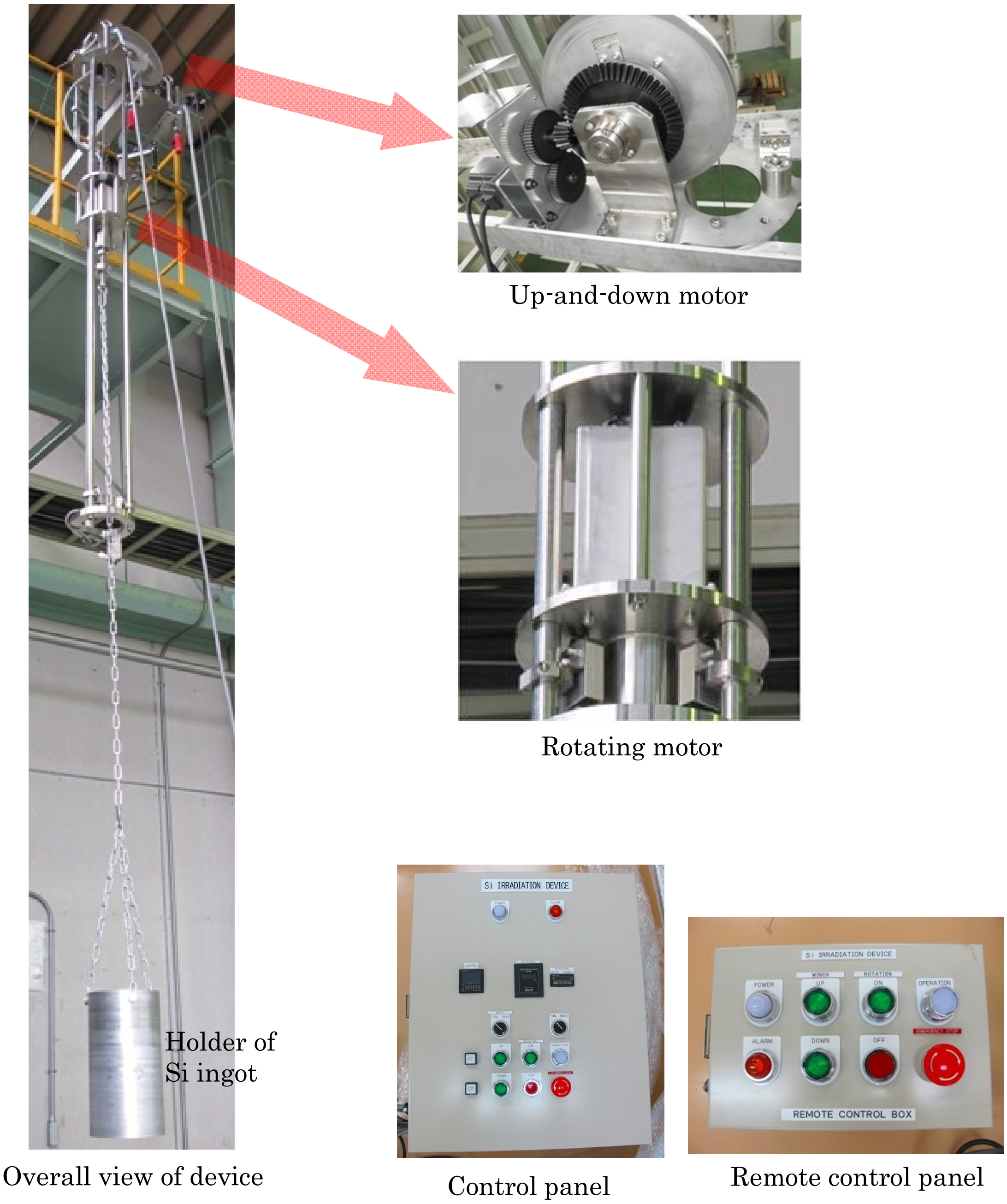

Fig.3 Photograph of Si-rotating device

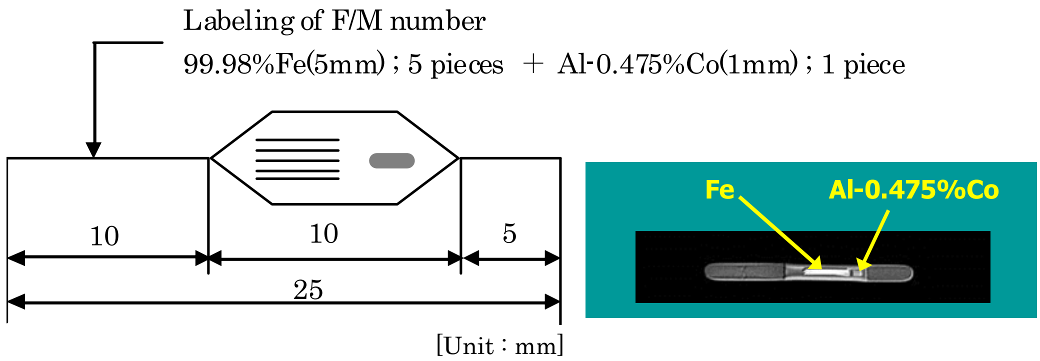

Fig.4 Structure of fluence monitor type I (F/M number 1 to 30)

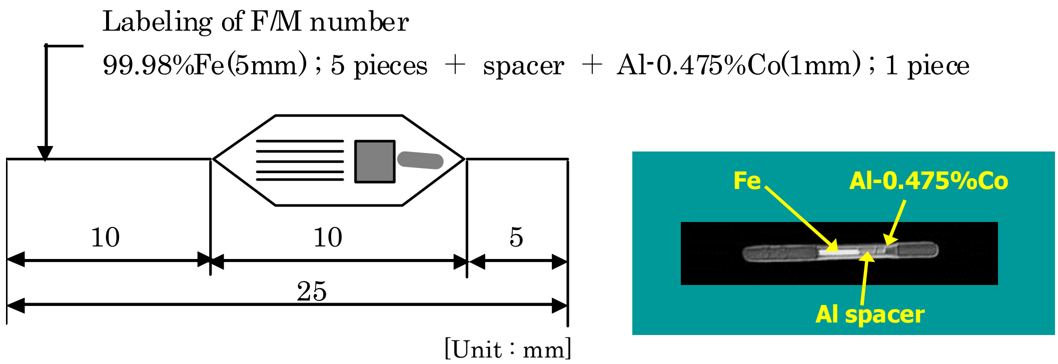

Fig.5 Structure of fluence monitor type II (F/M number 31 to 60)

Fig.6 Photograph of fluence monitor

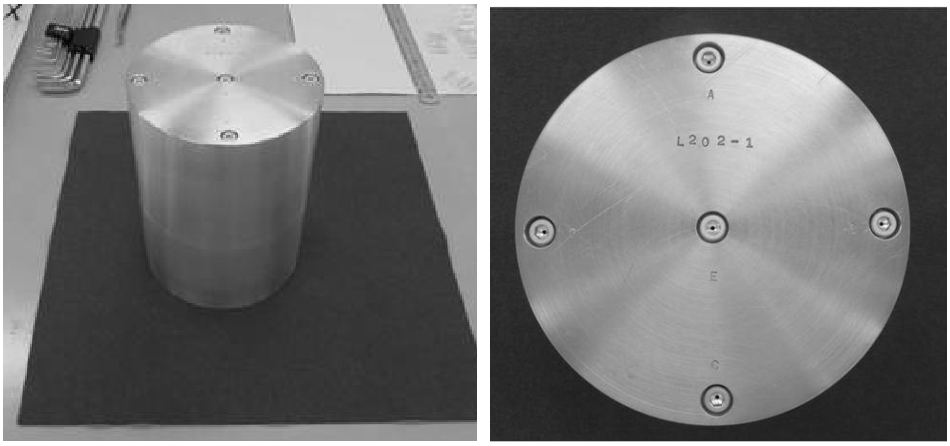

Fig.7　　Photograph of aluminum ingot

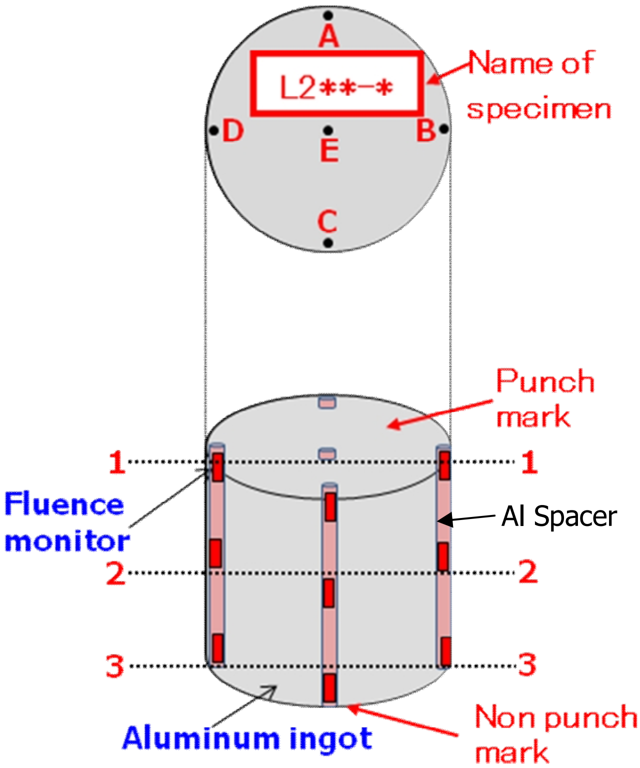

Fig.8　　Loading location of fluence monitor

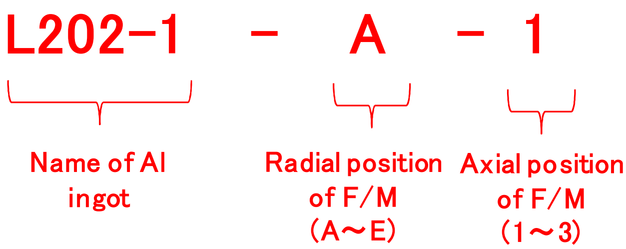

Fig.9　　Numbering method of loading location of fluence monitor

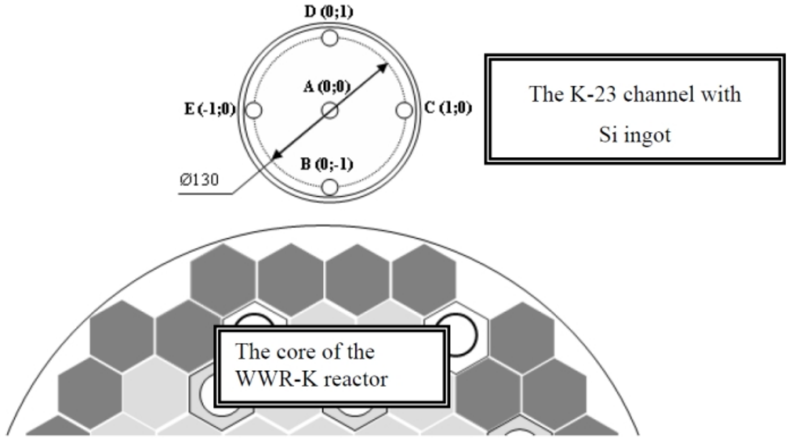

Fig.10 Layout of calculation nodes for silicon ingot

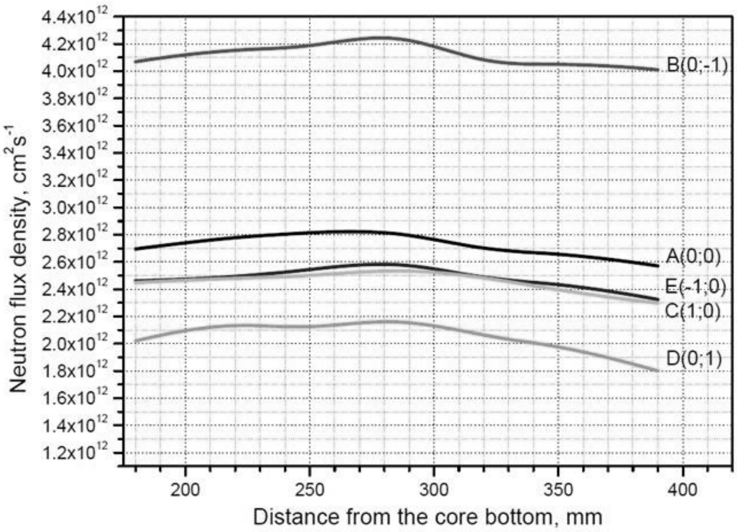

Fig.11 Distribution of thermal neutron flux density (E<0.465eV) for ϕ 152mm×L200mm silicon ingot

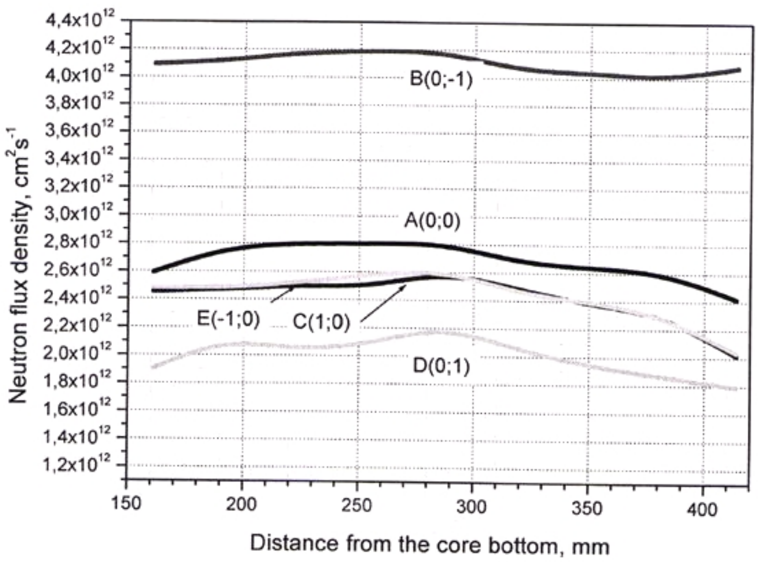

Fig.12 Distribution of thermal neutron flux density (E<0.465eV) for ϕ 152mm×L280mm silicon ingot

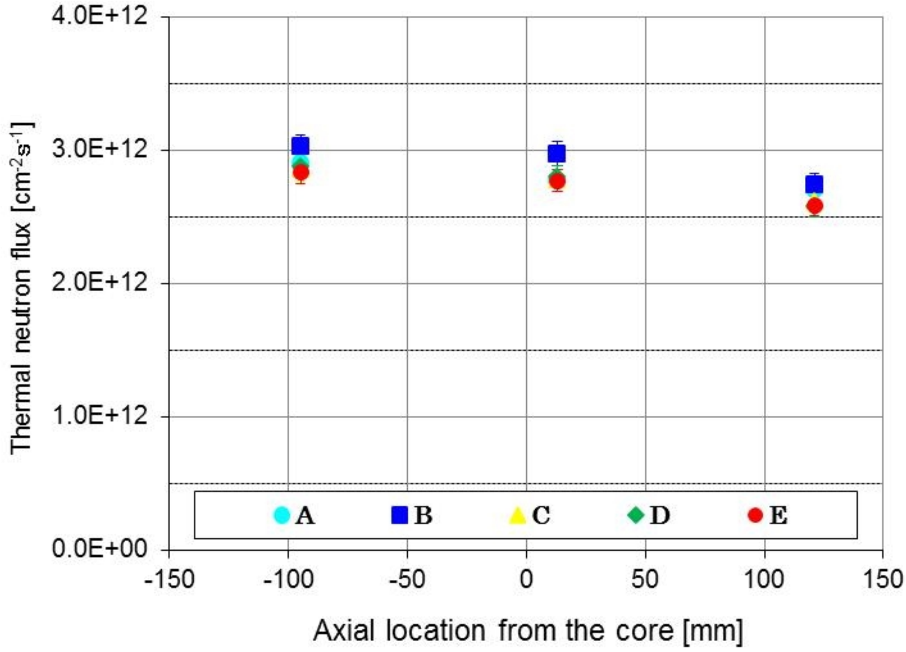

Fig.13 Distribution of thermal neutron flux density (E<0.683eV) by measurement of fluence monitors at L278-2 Al ingot

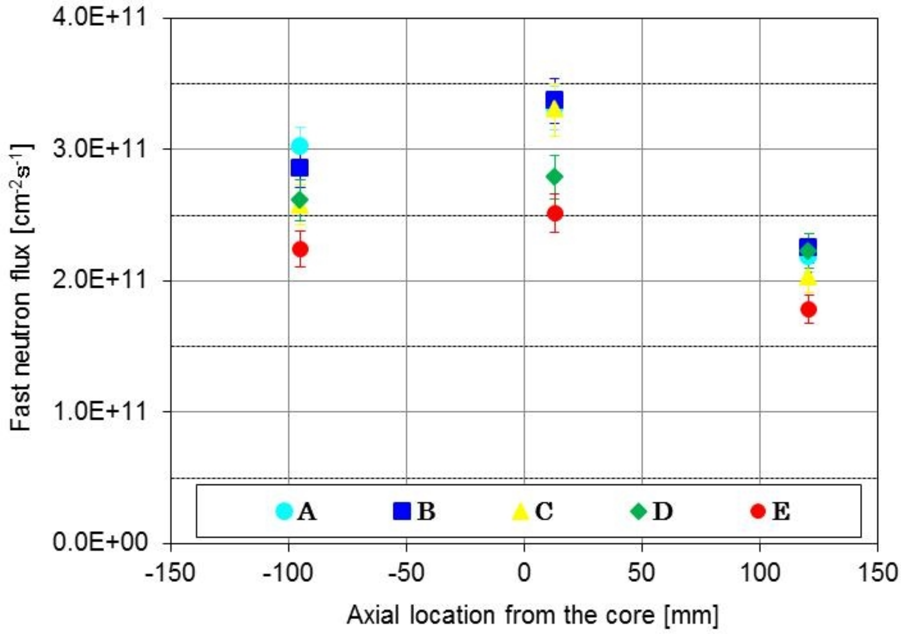

Fig.14 Distribution of fast neutron flux density (E > 1MeV) by measurement of fluence monitors at L278-2 Al ingot

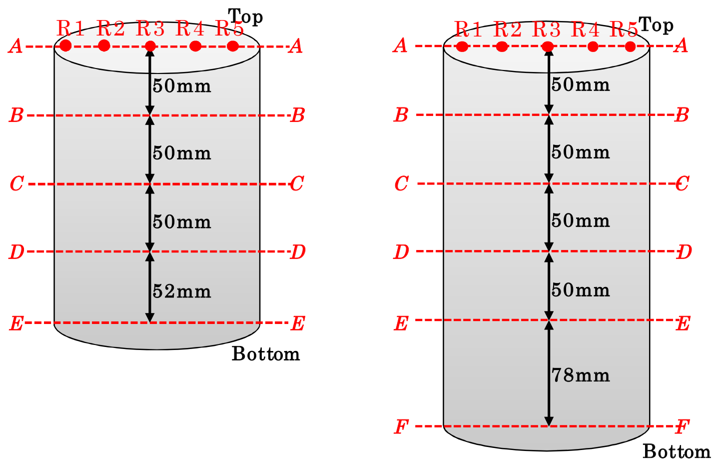

(1) Silicon ingot No.1
(φ151mm×202mmL)

(2) Silicon ingot No.2
(φ151mm×278mmL)

● ; Five measured points on each plane

Fig.15 Cutting location of irradiated silicon ingot for resistivity measurement

国際単位系（SI）

表１．SI 基本単位

基本量	SI 基本単位	
	名称	記号
長さ	メートル	m
質量	キログラム	kg
時間	秒	s
電流	アンペア	A
熱力学温度	ケルビン	K
物質量	モル	mol
光度	カンデラ	cd

表２．基本単位を用いて表されるSI組立単位の例

組立量	SI 組立単位	
	名称	記号
面積	平方メートル	m^2
体積	立方メートル	m^3
速さ，速度	メートル毎秒	m/s
加速度	メートル毎秒毎秒	m/s^2
波数	毎メートル	m^{-1}
密度，質量密度	キログラム毎立方メートル	kg/m^3
面積密度	キログラム毎平方メートル	kg/m^2
比体積	立方メートル毎キログラム	m^3/kg
電流密度	アンペア毎平方メートル	A/m^2
磁界の強さ	アンペア毎メートル	A/m
量濃度(a)，濃度	モル毎立方メートル	mol/m^3
質量濃度	キログラム毎立方メートル	kg/m^3
輝度	カンデラ毎平方メートル	cd/m^2
屈折率(b)	（数字の）1	1
比透磁率(b)	（数字の）1	1

(a) 量濃度（amount concentration）は臨床化学の分野では物質濃度（substance concentration）ともよばれる。
(b) これらは無次元量あるいは次元１をもつ量であるが、そのことを表す単位記号である数字の１は通常は表記しない。

表３．固有の名称と記号で表されるSI組立単位

組立量	SI 組立単位			
	名称	記号	他のSI単位による表し方	SI基本単位による表し方
平面角	ラジアン(b)	rad	1 (b)	m/m
立体角	ステラジアン(b)	sr(c)	1 (b)	m^2/m^2
周波数	ヘルツ(d)	Hz		s^{-1}
力	ニュートン	N		$m\ kg\ s^{-2}$
圧力，応力	パスカル	Pa	N/m^2	$m^{-1}\ kg\ s^{-2}$
エネルギー，仕事，熱量	ジュール	J	N m	$m^2\ kg\ s^{-2}$
仕事率，工率，放射束	ワット	W	J/s	$m^2\ kg\ s^{-3}$
電荷，電気量	クーロン	C		s A
電位差（電圧），起電力	ボルト	V	W/A	$m^2\ kg\ s^{-3}\ A^{-1}$
静電容量	ファラド	F	C/V	$m^{-2}\ kg^{-1}\ s^4\ A^2$
電気抵抗	オーム	Ω	V/A	$m^2\ kg\ s^{-3}\ A^{-2}$
コンダクタンス	ジーメンス	S	A/V	$m^{-2}\ kg^{-1}\ s^3\ A^2$
磁束	ウエーバ	Wb	Vs	$m^2\ kg\ s^{-2}\ A^{-1}$
磁束密度	テスラ	T	Wb/m^2	$kg\ s^{-2}\ A^{-1}$
インダクタンス	ヘンリー	H	Wb/A	$m^2\ kg\ s^{-2}\ A^{-2}$
セルシウス温度	セルシウス度(e)	℃		K
光束	ルーメン	lm	cd sr(c)	cd
照度	ルクス	lx	lm/m^2	$m^{-2}\ cd$
放射性核種の放射能(f)	ベクレル(d)	Bq		s^{-1}
吸収線量, 比エネルギー分与, カーマ	グレイ	Gy	J/kg	$m^2\ s^{-2}$
線量当量, 周辺線量当量, 方向性線量当量, 個人線量当量	シーベルト(g)	Sv	J/kg	$m^2\ s^{-2}$
酸素活性	カタール	kat		$s^{-1}\ mol$

(a)SI接頭語は固有の名称と記号を持つ組立単位と組み合わせても使用できる。しかし接頭語を付した単位はもはやコヒーレントではない。
(b)ラジアンとステラジアンは数字の１に対する単位の特別な名称で、量についての情報をつたえるために使われる。実際には、使用する時には記号rad及びsrが用いられるが、習慣として組立単位としての記号である数字の１は明示されない。
(c)測光学ではステラジアンという名称と記号srを単位の表し方の中に、そのまま維持している。
(d)ヘルツは周期現象についてのみ、ベクレルは放射性核種の統計的過程についてのみ使用される。
(e)セルシウス度はケルビンの特別な名称で、セルシウス温度を表すために使用される。セルシウス度とケルビンの単位の大きさは同一である。したがって、温度差や温度間隔を表す数値はどちらの単位で表しても同じである。
(f)放射性核種の放射能（activity referred to a radionuclide）は、しばしば誤った用語で”radioactivity”と記される。
(g)単位シーベルト（PV,2002,70,205）についてはCIPM勧告2（CI-2002）を参照。

表４．単位の中に固有の名称と記号を含むSI組立単位の例

組立量	SI 組立単位		
	名称	記号	SI 基本単位による表し方
粘度	パスカル秒	Pa s	$m^{-1}\ kg\ s^{-1}$
力のモーメント	ニュートンメートル	N m	$m^2\ kg\ s^{-2}$
表面張力	ニュートン毎メートル	N/m	$kg\ s^{-2}$
角速度	ラジアン毎秒	rad/s	$m\ m^{-1}\ s^{-1}=s^{-1}$
角加速度	ラジアン毎秒毎秒	rad/s^2	$m\ m^{-1}\ s^{-2}=s^{-2}$
熱流密度，放射照度	ワット毎平方メートル	W/m^2	$kg\ s^{-3}$
熱容量，エントロピー	ジュール毎ケルビン	J/K	$m^2\ kg\ s^{-2}\ K^{-1}$
比熱容量，比エントロピー	ジュール毎キログラム毎ケルビン	J/(kg K)	$m^2\ s^{-2}\ K^{-1}$
比エネルギー	ジュール毎キログラム	J/kg	$m^2\ s^{-2}$
熱伝導率	ワット毎メートル毎ケルビン	W/(m K)	$m\ kg\ s^{-3}\ K^{-1}$
体積エネルギー	ジュール毎立方メートル	J/m^3	$m^{-1}\ kg\ s^{-2}$
電界の強さ	ボルト毎メートル	V/m	$m\ kg\ s^{-3}\ A^{-1}$
電荷密度	クーロン毎立方メートル	C/m^3	$m^{-3}\ s\ A$
表面電荷	クーロン毎平方メートル	C/m^2	$m^{-2}\ s\ A$
電束密度，電気変位	クーロン毎平方メートル	C/m^2	$m^{-2}\ s\ A$
誘電率	ファラド毎メートル	F/m	$m^{-3}\ kg^{-1}\ s^4\ A^2$
透磁率	ヘンリー毎メートル	H/m	$m\ kg\ s^{-2}\ A^{-2}$
モルエネルギー	ジュール毎モル	J/mol	$m^2\ kg\ s^{-2}\ mol^{-1}$
モルエントロピー, モル熱容量	ジュール毎モル毎ケルビン	J/(mol K)	$m^2\ kg\ s^{-2}\ K^{-1}\ mol^{-1}$
照射線量（Ｘ線及びγ線）	クーロン毎キログラム	C/kg	$kg^{-1}\ s\ A$
吸収線量率	グレイ毎秒	Gy/s	$m^2\ s^{-3}$
放射強度	ワット毎ステラジアン	W/sr	$m^4\ m^{-2}\ kg\ s^{-3}=m^2\ kg\ s^{-3}$
放射輝度	ワット毎平方メートル毎ステラジアン	$W/(m^2\ sr)$	$m^2\ m^{-2}\ kg\ s^{-3}=kg\ s^{-3}$
酵素活性濃度	カタール毎立方メートル	kat/m^3	$m^{-3}\ s^{-1}\ mol$

表５．SI 接頭語

乗数	名称	記号	乗数	名称	記号
10^{24}	ヨタ	Y	10^{-1}	デシ	d
10^{21}	ゼタ	Z	10^{-2}	センチ	c
10^{18}	エクサ	E	10^{-3}	ミリ	m
10^{15}	ペタ	P	10^{-6}	マイクロ	µ
10^{12}	テラ	T	10^{-9}	ナノ	n
10^{9}	ギガ	G	10^{-12}	ピコ	p
10^{6}	メガ	M	10^{-15}	フェムト	f
10^{3}	キロ	k	10^{-18}	アト	a
10^{2}	ヘクト	h	10^{-21}	ゼプト	z
10^{1}	デカ	da	10^{-24}	ヨクト	y

表６．SIに属さないが、SIと併用される単位

名称	記号	SI 単位による値
分	min	1 min=60 s
時	h	1 h =60 min=3600 s
日	d	1 d=24 h=86 400 s
度	°	1°=(π/180) rad
分	’	1’=(1/60)°=(π/10 800) rad
秒	”	1”=(1/60)’=(π/648 000) rad
ヘクタール	ha	1 ha=1 $hm^2=10^4m^2$
リットル	L，l	1 L=1 l=1 $dm^3=10^3cm^3=10^{-3}m^3$
トン	t	1 t=10^3 kg

表７．SIに属さないが、SIと併用される単位で、SI単位で表される数値が実験的に得られるもの

名称	記号	SI 単位で表される数値
電子ボルト	eV	1 eV=1.602 176 53(14)×10^{-19}J
ダルトン	Da	1 Da=1.660 538 86(28)×10^{-27}kg
統一原子質量単位	u	1 u=1 Da
天文単位	ua	1 ua=1.495 978 706 91(6)×10^{11}m

表８．SIに属さないが、SIと併用されるその他の単位

名称	記号	SI 単位で表される数値
バール	bar	1 bar=0.1MPa=100 kPa=10^5Pa
水銀柱ミリメートル	mmHg	1 mmHg≈133.322Pa
オングストローム	Å	1 Å=0.1nm=100pm=10^{-10}m
海里	M	1 M=1852m
バーン	b	1 b=100$fm^2=(10^{-12}cm)^2=10^{-28}m^2$
ノット	kn	1 kn=(1852/3600)m/s
ネーパ	Np	SI単位との数値的な関係は、対数量の定義に依存。
ベル	B	
デシベル	dB	

表９．固有の名称をもつCGS組立単位

名称	記号	SI 単位で表される数値
エルグ	erg	1 erg=10^{-7} J
ダイン	dyn	1 dyn=10^{-5}N
ポアズ	P	1 P=1 dyn s cm^{-2}=0.1Pa s
ストークス	St	1 St =1$cm^2\ s^{-1}=10^{-4}m^2\ s^{-1}$
スチルブ	sb	1 sb =1cd $cm^{-2}=10^4$cd m^{-2}
フォト	ph	1 ph=1cd sr cm^{-2} =10^4lx
ガル	Gal	1 Gal =1cm $s^{-2}=10^{-2}ms^{-2}$
マクスウエル	Mx	1 Mx = 1G $cm^2=10^{-8}$Wb
ガウス	G	1 G =1Mx cm^{-2} =10^{-4}T
エルステッド(a)	Oe	1 Oe ≙ $(10^3/4\pi)$A m^{-1}

(a) ３元系のCGS単位系とSIでは直接比較できないため、等号「 ≙ 」は対応関係を示すものである。

表10．SIに属さないその他の単位の例

名称	記号	SI 単位で表される数値
キュリー	Ci	1 Ci=3.7×10^{10}Bq
レントゲン	R	1 R = 2.58×10^{-4}C/kg
ラド	rad	1 rad=1cGy=10^{-2}Gy
レム	rem	1 rem=1 cSv=10^{-2}Sv
ガンマ	γ	1 γ=1 nT=10^{-9}T
フェルミ		1フェルミ=1 fm=10^{-15}m
メートル系カラット		1メートル系カラット= 0.2 g = 2×10^{-4}kg
トル	Torr	1 Torr = (101 325/760) Pa
標準大気圧	atm	1 atm = 101 325 Pa
カロリー	cal	1 cal=4.1858J（「15℃」カロリー），4.1868J（「IT」カロリー），4.184J（「熱化学」カロリー）
ミクロン	µ	1 µ =1µm=10^{-6}m

（第8版，2006年）